



## STRONG GROUND MOTION SIMULATION IN OSAKA BASIN, JAPAN, FOR THE 2018 NORTHERN OSAKA PREFECTURE EARTHQUAKE

H. Sekiguchi<sup>(1)</sup>, K. Asano<sup>(2)</sup>, T. Iwata<sup>(3)</sup>

<sup>(1)</sup> Associate Professor, Disaster Prevention Research Institute, Kyoto University, [sekiguchi.haruko.6u@kyoto-u.ac.jp](mailto:sekiguchi.haruko.6u@kyoto-u.ac.jp)

<sup>(2)</sup> Associate Professor, Disaster Prevention Research Institute, Kyoto University, [k-asano@egmdpri01.dpri.kyoto-u.ac.jp](mailto:k-asano@egmdpri01.dpri.kyoto-u.ac.jp)

<sup>(3)</sup> Professor, Disaster Prevention Research Institute, Kyoto University, [iwata@egmdpri01.dpri.kyoto-u.ac.jp](mailto:iwata@egmdpri01.dpri.kyoto-u.ac.jp)

### Abstract

An  $M_w$  5.5 earthquake occurred at 13 km depth under the Osaka Basin, Japan, on June 18, 2018. Observed ground motions in the Osaka Basin exhibited a complex wavefield following the arrival of the direct S-wave due to the three-dimensional structure of the sedimentary layers of the basin. We conduct a ground motion simulation with a finite source model for this earthquake using three-dimensional velocity structure models of the Osaka and Nara sedimentary basins to investigate the strong motion generation mechanism and to validate the three-dimensional basin structure models. The three-dimensional Osaka sedimentary basin model has been constructed following the strategy of constructing a depth model of isochronous surfaces and converting the depositional age structure into the seismic wave-velocity structure employed in a former model, summarizing depth data of key horizons from the reflection surveys, borehole investigations, PS-P travel time difference data from the strong motion observations, and the surface-wave predominant frequency from the horizontal-to-vertical spectral ratio of microtremor observations. Ground motion is calculated up to 2 Hz using the three-dimensional finite difference method for the three-dimensional sedimentary structure for  $V_s > 350$  m/s and the equivalent linear method for the Holocene and Pleistocene deposits. Peak ground velocity distribution of the simulation shows large values distributed southwest of the epicenter, which agrees with the observed distribution. This feature is due to the S-wave radiation pattern of the northeast-to-southwest striking fault plane, one of the two fault planes comprising the coseismic fault, enhanced by the rupture propagation toward the southwest-updip on this fault plane, and further raised by the amplification effect of the sedimentary layers. The calculated ground motion shows a complex wavefield in which waves are generated in the basin after the arrival of the direct wave and propagate in various directions. Calculated arrivals of the later phases are in agreement with the observed waveforms. The later phases are the multiple reflections between the surface and the basin bedrock or the surface waves generated at the basin edge or the step-like bedrock topography under the sediment due to the active faults. The later phases sometimes have larger amplitude than those of the direct S-waves, depending on the time and location. Our results show that the three-dimensional sedimentary basin model has high ability to reproduce the ground motion up to 2 Hz. However, there are sites where the reproduction is not successful, particularly near the basin edge. Poor-fit stations were also seen far from the epicenter and near the step-like bedrock topography. The Q-factor of the sediment is examined by fitting the velocity envelope of the later phases. We obtain  $Q = 0.45V_s$  in 0.1–0.5 Hz,  $Q = 0.26V_s$  in 0.5–1.0 Hz, and  $Q = 0.15V_s$  in 1.0–2.0 Hz, where  $V_s$  is the S-wave velocity (m/s), indicating a decreasing Q with increasing frequency in this range.

*Keywords: ground motion simulation; sedimentary layer; Osaka Basin; the 2018 Northern Osaka Prefecture earthquake; finite difference method*



## 1. Introduction

The 2018 Northern Osaka Prefecture earthquake (2018 June 18 07:58 JST) was not a big earthquake ( $M_w$  5.5) but caused strong motion in nearby Osaka and Kyoto basins. Peak ground velocities (PGVs) exceeding 40 cm/s were observed up to 10 km from the epicenter (Fig.1), and the seismic intensity reached lower 6 on the Japanese seven-stage seismic scale. The coseismic fault is located under a densely populated area. The earthquake caused a lot of building damage and elevator traps. The paralysis of public transportation yielded many stranded people.

More than 70 strong motion stations in the Osaka basin recorded the ground motion of this earthquake (Fig.1). The observed waveforms in the Osaka basin have complex later phases after the direct waves, which are considered to be generated in the sediment of the basin (Fig.2). The later phases sometimes have larger amplitudes than the direct waves (Fig.2).

The velocity structure of the Osaka sedimentary basin has been extensively modeled and revised since the 1990s [1–9] for use in evaluation of the seismic response of the basin and prediction of ground motion for anticipated future great earthquakes.

In this study, we perform a ground motion simulation of the 2018 Northern Osaka Prefecture earthquake with the latest velocity structure model [9] of the basin, examine the performance of the velocity structure model, and analyze the ground motion generation mechanism of the basin. The earthquake is not small and occurred beneath the basin, which enables us to examine the response of the basin in a fairly wide frequency range (0.1–2.0 Hz) without needing to take into account the velocity structure outside the basin.

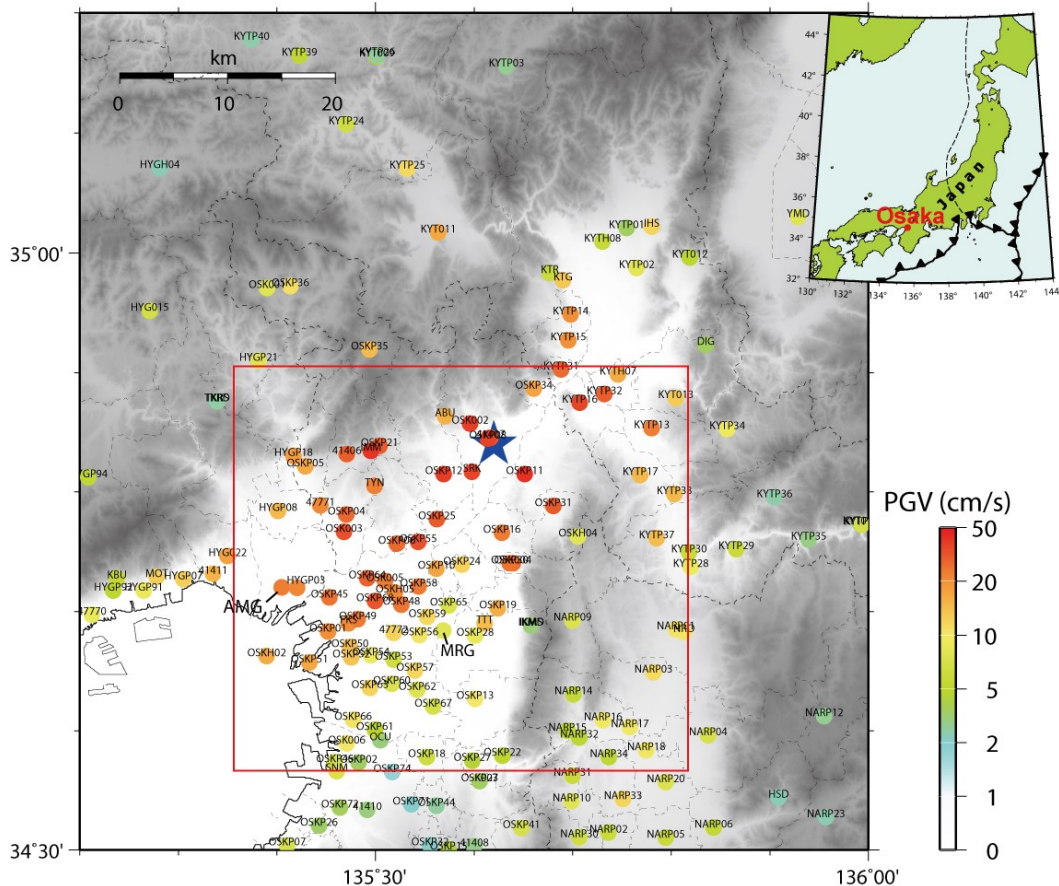


Fig. 1 – Observed peak ground velocity (PGV) distribution. The blue star indicates the epicenter of the earthquake. The red rectangle indicates the area of ground motion simulation.

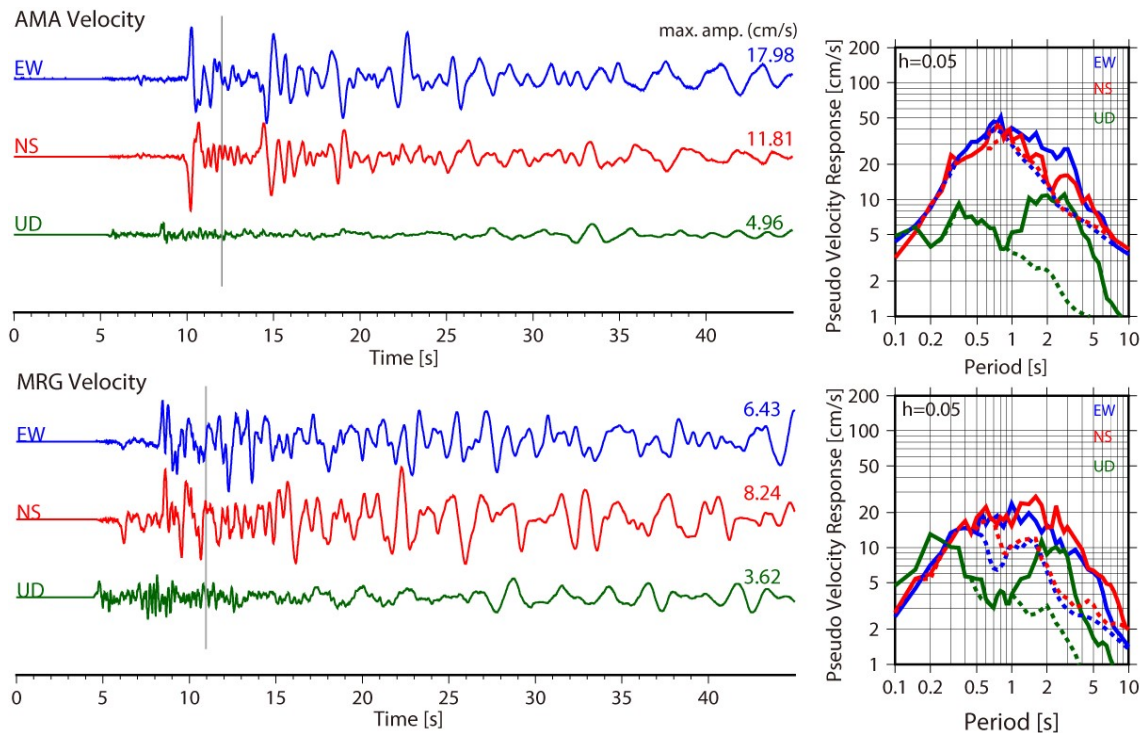


Fig. 2 – Observed velocity waveforms and their pseudo velocity response spectra at sites AMA and MRG. Dashed lines indicate spectra for waves prior to the end of the direct S-wave (up to time indicated by the gray lines on the waveforms).

## 2. Ground motion simulation

Ground motion is calculated in the 0.1–2.0 Hz range using the three-dimensional finite difference method (FDM) [10] for the three-dimensional crustal and sedimentary structure of S-wave velocity ( $V_s$ ) larger than 350 m/s and using the equivalent linear method [11] for the Holocene and Pleistocene deposits [12].

In the FDM simulation, the medium with  $V_s < 350$  m/s in the velocity structure model is replaced by the medium with  $V_s = 350$  m/s. The grid interval is 25 m along the horizontal axes, 25 m down to 3 km depth, and greater than that elsewhere along the vertical axis according to the medium S-wave velocity. An inelastic attenuation effect is included in the form of a linear frequency-dependent Q operator, following the method proposed by [13].

The source model used in the FDM simulation is one derived with the waveform inversion in 0.1–2.0 Hz [14]. The source model has two fault planes, a north-south-trending thrust fault (F1) and a northeast-southwest trending dextral strike-slip fault (F2) located south of F1. The rupture initiated on F1 and started on F2 0.3 s later. The moment release on F2 is larger than that on the other fault. The slip vectors and the rupture propagation of the source model focus the maximum forward directivity effect in the southwest-updip direction from F2.

The three-dimensional velocity structure model used in the FDM simulation combines the Osaka basin model [9], the Nara basin model [15], and the crustal part of the Japan Integrated Velocity Structure Model [16]. The Osaka sedimentary basin model [9] has been constructed following the modeling strategy of constructing a depth model of an isochronous surfaces and converting the depositional age structure into the seismic-wave-velocity structure employed in former models [5, 6], summarizing depth data of key horizons from the reflection surveys, borehole investigations, PS-P travel time difference data from the strong motion observations, and the surface-wave predominant frequency data from the horizontal-to-vertical spectral ratio of microtremor observations. The survey and analysis data obtained under a Japanese Ministry of Education, Culture, Sports, Science, and Technology (MEXT) contract research project titled “Comprehensive Research



on the Uemachi Fault Zone” [17] was included. The Nara basin model [15] has been constructed with the same modeling strategy from the bedrock depth distribution model based on gravity anomaly, borehole data, and the surface-wave predominant frequency from the horizontal-to-vertical spectral ratio of dense microtremor observation.

The Q-factor in the FDM simulation is the same as the one used in [18] that estimated appropriate Q-factors for the sediments in the Osaka basin with the FDM simulation in the 0.05–0.5 Hz range under the formulation of [13]. It may not be appropriate to adopt this Q-factor in our simulation because our target frequency range is different (0.1–2 Hz). Therefore, we examine the Q-factor setting later.

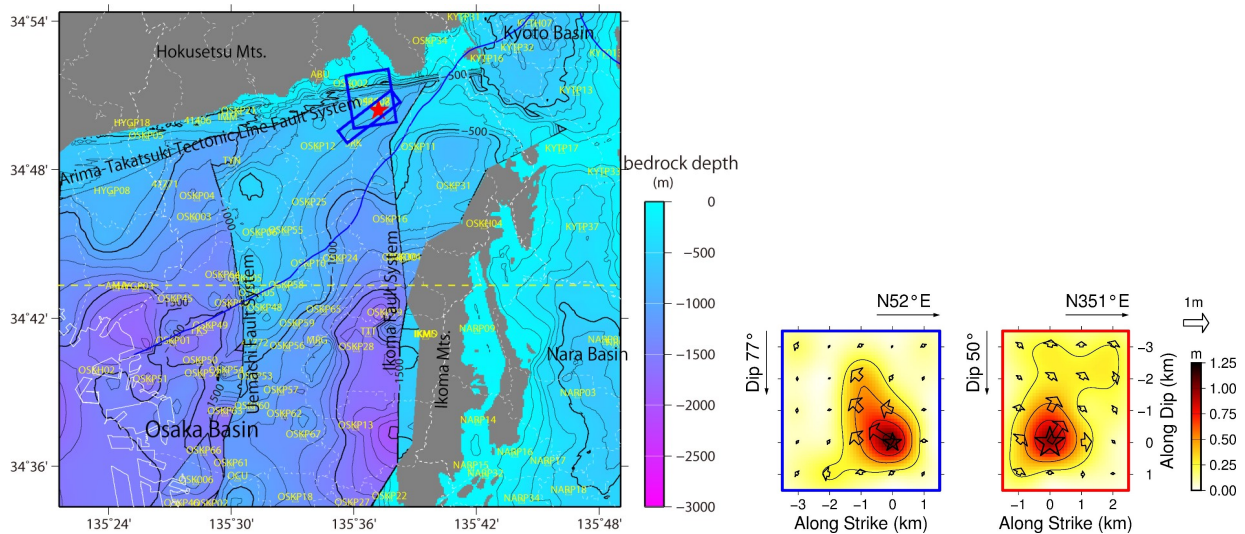


Fig. 3 – Left: Bedrock depth distribution of the three-dimensional velocity structure model. Blue rectangles indicate the two fault planes of the source model [14] projected onto the earth surface. The yellow dashed line indicates the line along which calculated waveforms are shown in Fig.6. Right: Slip distributions on the fault planes of the source model [14].

### 3. Results

PGV distribution of the calculated ground motion shows large values to the southwest of the epicenter, which agrees with the observed distribution (Fig.4). This feature is due to the compound effect of the S-wave radiation pattern of the northeast-southwest striking fault plane (F2), the rupture propagation toward the southwest-updip direction on this fault plane, and the amplification by the sedimentary layers. Locally large PGV is found along the margin of the basin, along the faults in the basin, and near the hollows of the bedrock surface. This is due to the constructive interference of the seismic wave whose wavefront is largely deformed at the curved or step-like bedrock surface. Overall, the calculated PGV distribution agrees with the observation.

The calculated ground motion shows a complex wavefield in which a lot of later phases emerge from various places in the basin after the arrival of the direct wave and propagate in various directions (Fig.5). Analyzing the propagation of the later phases at depth, we find that they involve the multiple reflections between the surface and the basin bedrock or the surface waves generated at the basin edge or the step-like bedrock topography under the sediment due to the active faults. The later phases sometimes have larger amplitudes than the direct S-waves. One example is the ground motion at MRG (Fig.2). MRG has a relatively small direct wave because it is located near the minimum of the S-wave radiation pattern from F2. However, the direct S-wave at the maximum of the forward directivity hits the earth surface directed toward the south, while multiple reflections (Fig.5) produce relatively large later phases at MRG.

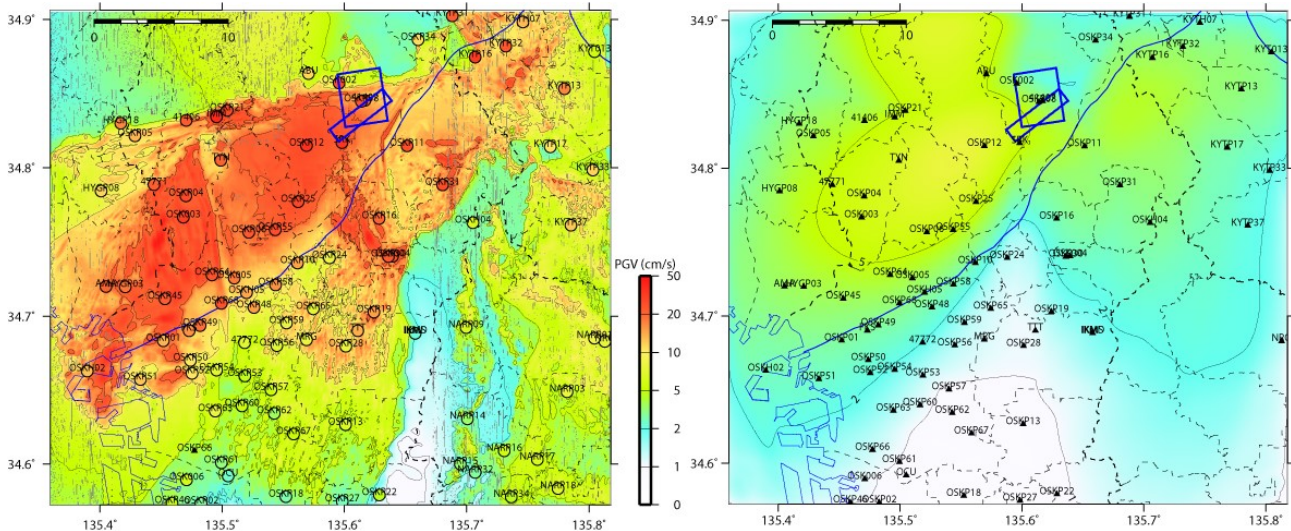


Fig. 4 – PGV (vector summation of the three components) distribution of the calculated ground motion. Left: The ground motion simulation with sedimentary layers. Colors in circles at observation sites indicate the observed PGV. Right: The ground motion simulation without sedimentary layers.

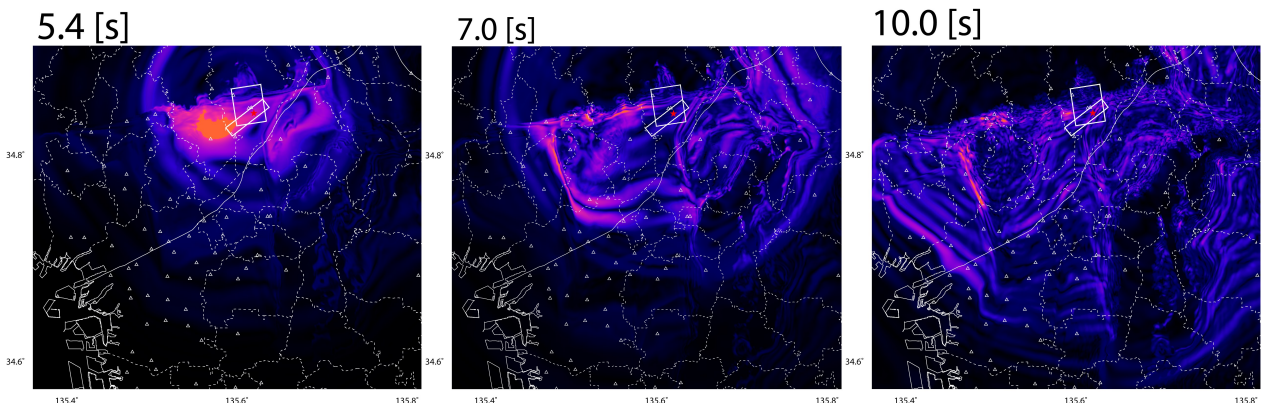


Fig. 5 – Snapshots of ground velocity (vector summation of the three components) of the calculated ground motion.

Arrivals of the later phases are in agreement with the observed waveforms (Fig.6). However, the correspondence of the observed and synthetic waveforms gets worse as the time proceeds. The later the arrival of waves is, the more complicated the path of the waves from the source to the site. We see cases where a strong later phase travels in a direction shifted from the desired direction (compare waves near AMG, HYGP03, and OSKP45 in Fig.6). We can see the possibility of further tuning of the velocity structure model. On average, the amplitudes of the calculated waveforms underestimate the observation for the direct wave portion but overestimate it for the later phases. Moreover, the later the arrival of waves is, the richer they are in high-frequency components compared to the observation. The correlation between the observed and calculated waveforms is judged with the goodness-of-fit criterion by [19] (Figs.7, 8). Most of the stations in the Osaka basin earn a rating of fair or poor judgment. Poor-fit stations can often be seen at large distances from the epicenter and near the step-like bedrock topography.

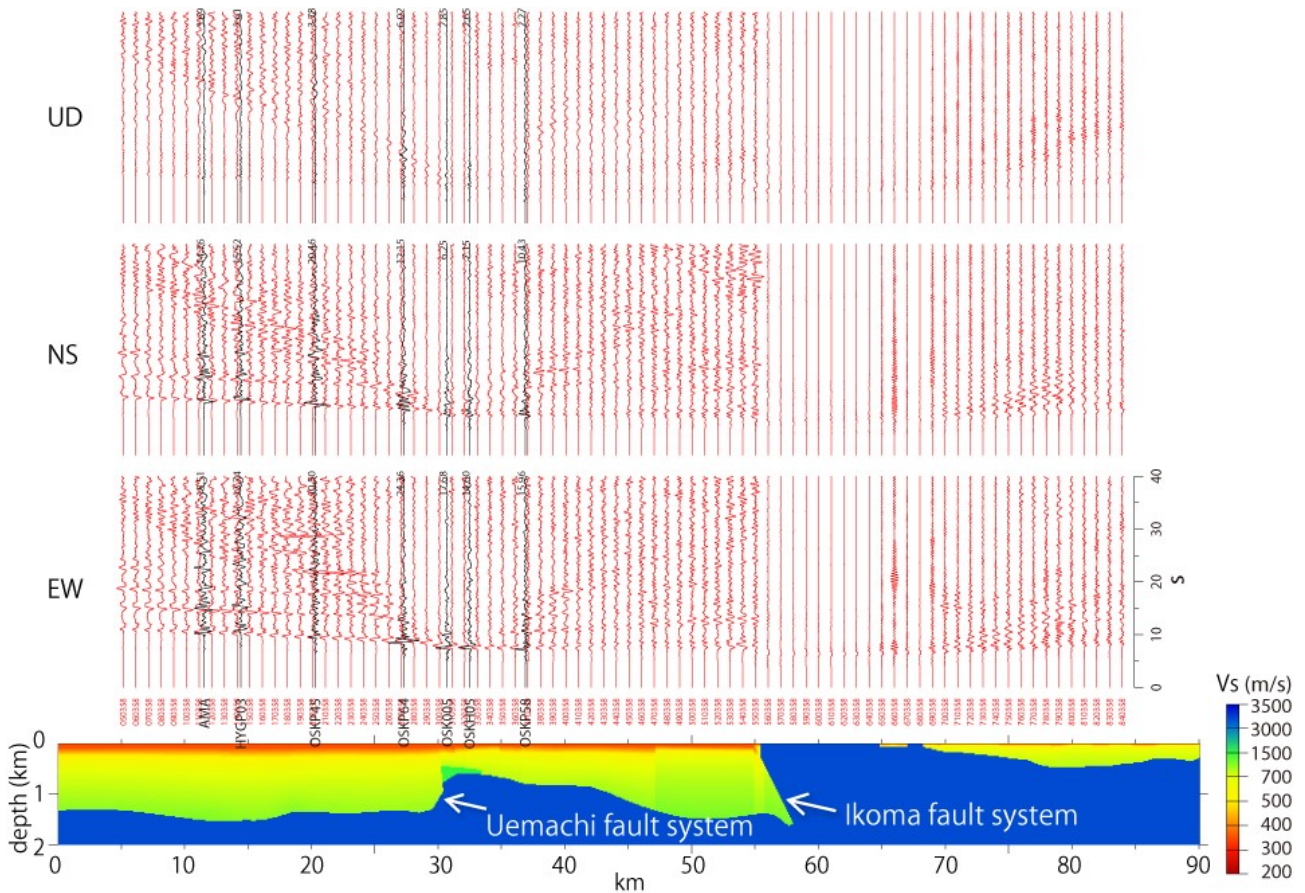


Fig. 6 – Upper: The calculated ground motion (red lines) along an east-west line passing AMG shown as a yellow dashed line in in Fig.3 and the observed ground motion near the line (black lines). Lower: S-wave velocity-depth profile below the line.

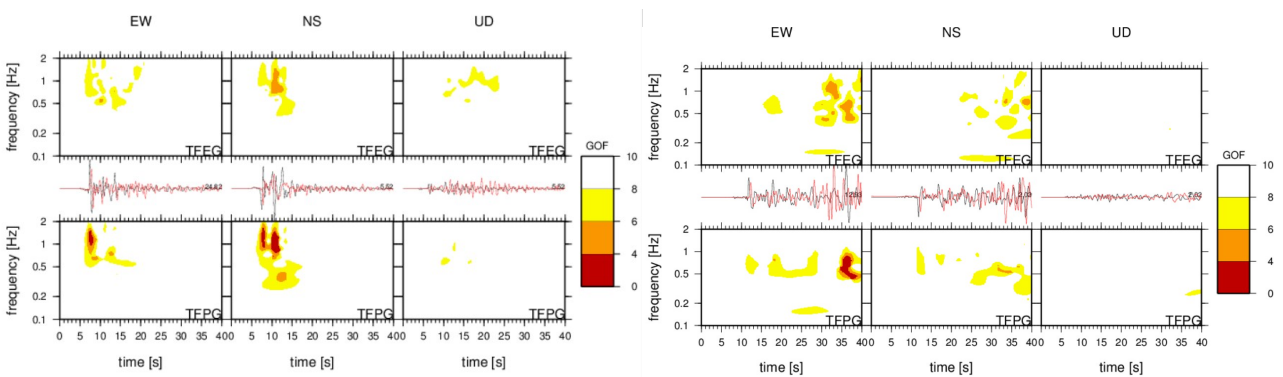


Fig. 7 – Goodness of fit evaluation [19] at OSKP04 (left) and OSKH02 (right). Waveforms in the middle are of the observation (black) and the simulation (red). Frames above each waveform are the globally normalized time-frequency envelope goodness-of-fits (TFEF) between the observed and calculated waveforms. Frames below each waveforms are the globally normalized time-frequency phase goodness-of-fits (TFPG) between the observed and calculated waveforms.

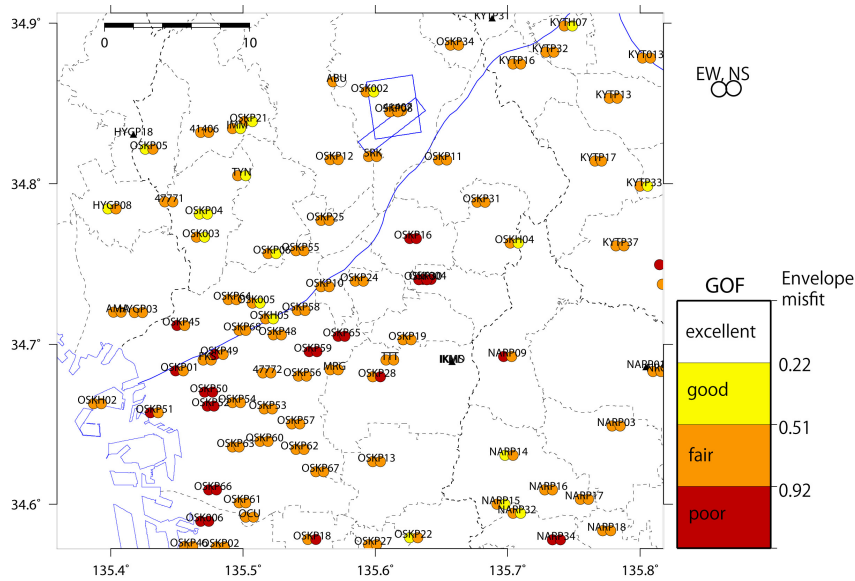


Fig. 8 – Envelope goodness-of-fits (frequency-time average of time-frequency envelope goodness-of-fit (TFEG)) distribution.

#### 4. Examination of Q-factor

From the feature that later phases of the calculated waveforms overestimate the observation and have richer high-frequency content, we explore a better setting for the Q-factor. We adopt the formulation of [13]

$$A = \exp\left[\frac{-\pi f_0 t}{Q_0}\right], \quad (1)$$

which means that the Q-factor for the other frequency becomes

$$Q = \frac{f}{f_0} Q_0. \quad (2)$$

The exploration of Q-factor setting is conducted as follows. We assume  $Q_0 = \alpha V_s$  as [14] did and perform FDM simulation with various  $\alpha$  values fixing  $f_0 = 0.2$  Hz. We band-pass filter the calculated waveforms in three narrow frequency ranges: 0.1–0.5, 0.5–1.0, and 1.0–2.0 Hz. We find the best  $\alpha$  value for each site and each frequency range that gives the smallest square sum of the residual between the observed and calculated RMS velocity envelopes in the time range from 20 s and 60 s after the origin time. An  $\alpha$  value of 0.1 with  $f_0 = 0.2$  corresponds to the attenuation setting adopted in [20] (Fig.9). The best  $\alpha$  value varies spatially and with frequency (Fig.10). The  $\alpha$  value most frequently found in the central part of the Osaka basin is 0.3 in 0.1–0.5 Hz, 0.07 in 0.5–1.0 Hz, and 0.02 in 1.0–2.0 Hz, which can be converted to  $Q = 0.45V_s$  in 0.1–0.5 Hz,  $Q = 0.26V_s$  in 0.5–1.0 Hz, and  $Q = 0.15V_s$  in 1.0–2.0 Hz if we use the center frequency of each frequency range. The Q-factor becomes smaller as the frequency increases in the range between 0.1 and 2.0 Hz, although the difference is a factor of about 3.

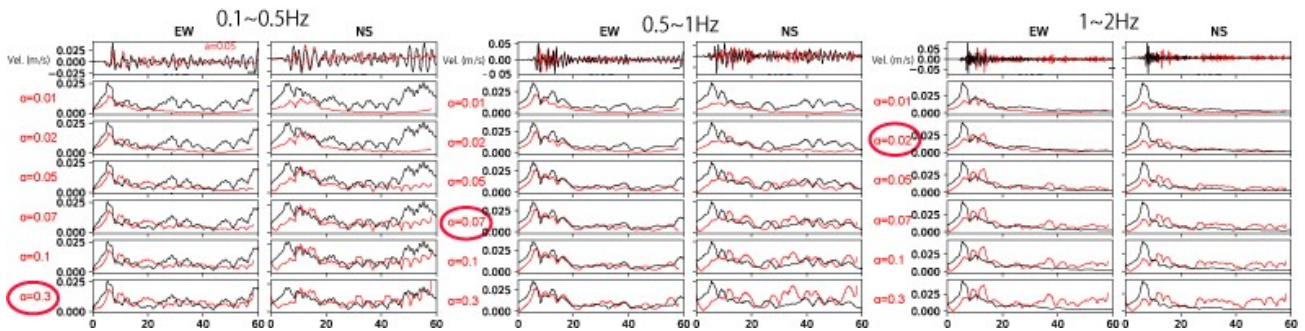


Fig. 9 – Comparison of RMS envelopes of observed and calculated ground motions at OSKP58.

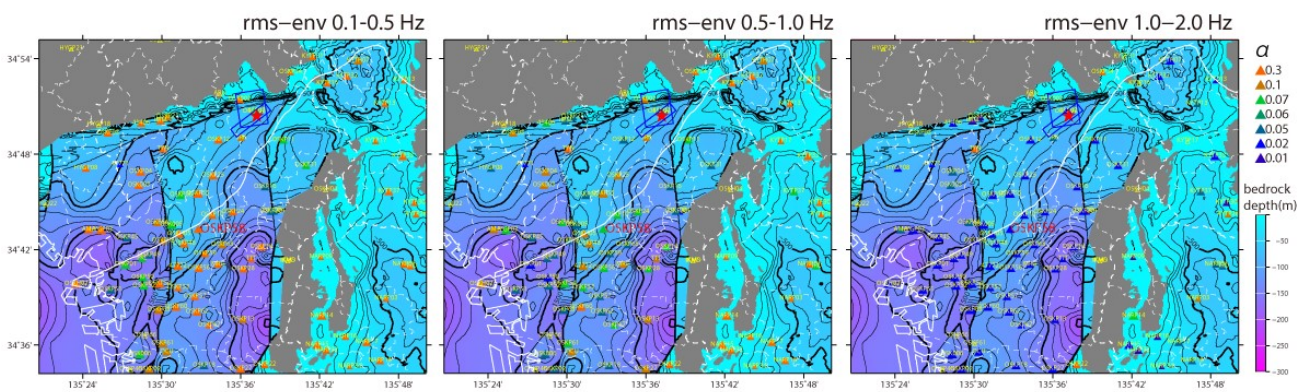


Fig. 10 – Best  $\alpha$  values at the observation sites in three different frequency ranges.

## 5. Conclusion

We performed a ground motion simulation of the 2018 Northern Osaka Prefecture earthquake with the latest velocity structure model of the Osaka basin, examined the performance of the velocity structure model, and analyzed the mechanism of the ground motion generation in the basin.

PGV distribution of the simulation shows large values to the southwest of the epicenter, which agrees with the observed distribution. This feature is due to the S-wave radiation pattern of the northeast to southwest striking fault plane enhanced by the rupture propagation toward the southwest-updip direction, and is further raised by amplification by the sedimentary layers. Locally large PGV is found along the margin of the basin, along the faults in the basin, and near the hollows of the bedrock surface. This is due to the constructive interference of the seismic wave whose wavefront is largely deformed at the curved or step-like bedrock surface.

The calculated ground motion shows a complex wavefield containing multiple reflection waves between the surface and the basin bedrock or the surface waves generated at the basin edge or the step-like bedrock topography under the sediment due to the active faults. Arrivals of the later phases were in agreement with the observed waveforms. Our results show that the three-dimensional sedimentary basin model has a high ability to reproduce the ground motion up to 2 Hz. The matches between the observed and calculated waveforms were fair or poor based on the goodness-of-fit criterion by [18]. Poor-fit stations were seen at large distances from the epicenter and near the step-like bedrock topography.

We examined the Q value of the sediment by fitting the velocity envelope from 20 s and 60 s after the origin time. We obtained  $Q = 0.45V_s$  in 0.1–0.5 Hz,  $Q = 0.26V_s$  in 0.5–1.0 Hz, and  $Q = 0.15V_s$  in 1.0–2.0 Hz, indicating that Q decreases with increasing frequency in this range.



## 6. Acknowledgements

The strong motion data were provided from the K-NET and KiKnet operated by the National Research Institute for Earth Science and Disaster Resilience, Japan Meteorological Agency, Osaka Prefecture, Hyogo Prefecture, Kyoto Prefecture, Nara Prefecture, the Committee of Earthquake Observation and Research in the Kansai Area, Institute for Integrated Radiation and Nuclear Science of Kyoto University, and Disaster Prevention Research Institute of Kyoto University. We used the Japan Integrated Velocity Structure Model Version 1 [16] to construct the crustal part of the three-dimensional velocity structure model. We used Generic Mapping Tools [21] to draw the figures. This work was partially supported by the Earthquake and Volcano Hazards Observation and Research Program of MEXT.

## 6. References

- [1] Kagawa T, Sawada S, Iwasaki Y, Nanjo J (1993): Modeling the deep sedimentary structure in the Osaka basin. *Proceedings of the 22nd JSCE Earthquake Engineering Symposium*, 199–202 (in Japanese).
- [2] Miyakoshi K, Kagawa T, Sawada S, Echigo T, Horie K (1997): Modeling the deep sedimentary structure in the Osaka Basin (2). *Proceedings of the 24th JSCE Earthquake Engineering Symposium*, 33–36 (in Japanese).
- [3] Miyakoshi K, Kagawa T, Zhao B, Tokubayashi T, Sawada S (1999): Modeling the deep sedimentary structure in the Osaka Basin (3). *Proceedings of the 25th JSCE Earthquake Engineering Symposium*, 185–188 (in Japanese).
- [4] Kagawa T, Zhao B, Miyakoshi K, Irikura K (2004): Modeling of 3D basin structures for seismic wave simulations based on available information on the target area: case study of the Osaka basin, Japan. *Bulletin of the Seismological Society of America*, **94**, 1353–1368. <https://doi.org/10.1785/012003165>
- [5] Horikawa H, Mizuno K, Ishiyama T, Satake K, Sekiguchi H, Kase Y, Sugiyama Y, Yokota H, Suehiro M, Yokokura T, Iwabuchi H, Kitada H, Pitarka A (2003): A three-dimensional subsurface structure model beneath the Osaka sedimentary basin, southwest Japan, with fault-related structural discontinuities. *Annual Report on Active Fault and Paleoseismicity Research, Geological Survey of Japan/AIST*, **3**, 225–259 (in Japanese with English abstract).
- [6] Osaka Prefecture (2005): *Fiscal Year 2004 Report of Investigation of the Underground Structure Beneath Osaka Plain* (in Japanese).
- [7] Iwata T, Kagawa T, Petukhin A, Ohnishi Y (2008): Basin and crustal velocity structure models for the simulation of strong ground motions in the Kinki area, Japan. *Journal of Seismology*, **12**, 223–234. <https://doi.org/10.1007/s10950-007-9086-7>
- [8] Iwaki A, Iwata T (2011): Estimation of three-dimensional boundary shape of the Osaka sedimentary basin by waveform inversion. *Geophysical Journal International*, **186**, 1255–1278. <https://doi.org/10.1111/j.1365-246X.2011.05102.x>
- [9] Sekiguchi H, Asano K, Iwata T, Yoshimi M, Horikawa H, Saomoto H, Hayashida T (2016): Construction of a 3D velocity structure model of Osaka sedimentary basin. *5th IASPEI / IAEE International Symposium: Effective Surface Geology Seismic Motion*, P103B.
- [10] Pitarka A (1999): 3D elastic finite-difference modeling of seismic motion using staggered grids with nonuniform spacing, *Bulletin of the Seismological Society of America*, **89**, 54–68.



- [11] Yoshida N, Suetomi I (1996): DYNEQ: A program for seismic response of layered structure based on equivalent linear methodology. *Sato Kogyo Engineering Laboratory Report*, 61–70 (in Japanese).
- [12] Yoshida K, Yamamoto K, Sekiguchi H (2006): Developing of a shallow sedimentary structure model for strong-motion predictions in the Osaka sedimentary basin. *Annual Report on Active Fault and Paleoequake Research, Geological Survey of Japan*, **6**, 123–141 (in Japanese with English abstract).
- [13] Graves RW (1996): Simulating seismic wave propagation in 3D elastic media using staggered-grid finite differences, *Bulletin of the Seismological Society of America*, **86**, 1091–1106.
- [14] Asano K, Iwata T, Hallo M (2018): Rupture process of the 2018 Northern Osaka earthquake ( $M_w$  5.6), an earthquake involving both thrust and strike-slip faults near a junction of major active fault systems surrounding the Osaka basin, Japan. AGU Fall Meeting, Washington, DC, USA.
- [15] Sekiguchi H, Asano K, Iwata T (2019): Three-dimensional velocity structure model of Nara Basin. *Journal of the Geological Society of Japan*, **125** (10), 715–730. <https://doi.org/10.5575/geosoc.2018.0053>
- [16] Koketsu K, Miyake H, Suzuki H (2012): Japan Integrated Velocity Structure Model Version 1. *The 15th World Conference on Earthquake Engineering*, Lisbon, Portugal.
- [17] Research and Development Bureau, Ministry of Education, Culture, Sports, Science and Technology and Disaster Prevention Research Institute, Kyoto University (2013): *Fiscal Year 2010–2012 Report of Integrated Research Project for the Uemachi Active Fault System*, 449p. (in Japanese).
- [18] Asano K, Sekiguchi H, Iwata T, Yoshimi M, Hayashida T, Saomoto H, Horikawa H (2016): Modelling of wave propagation and attenuation in the Osaka sedimentary basin, western Japan, during the 2013 Awaji Island earthquake. *Geophysical Journal International*, **204** (3), 1678–1694. <https://doi.org/10.1093/gji/ggv543>
- [19] Kristeková M, Kristek J, Moczo P (2009): Time-frequency misfit and goodness-of-fit criteria for quantitative comparison of time signals. *Geophysical Journal International*, **178** (2), 813–825. <https://doi.org/10.1111/j.1365-246X.2009.04177.x>
- [20] Kawabe H, Kamae K (2008): Prediction of long-period ground motions from huge subduction earthquakes in Osaka, Japan. *Journal of Seismology*, **12** (2), 173–184. <https://doi.org/10.1007/s10950-008-9089-z>
- [21] Wessel P, Smith WHF (1998): New, improved version of the Generic Mapping Tools released. *EOS Transactions AGU*, **79**, 579. <https://doi.org/10.1029/98EO00426>